Broadband photochromic effect and photoluminescence modulation in rare-earth-doped (Pb,La)(Zr,Ti)O_3 ceramics

Long Xu (许 龙)[1], Ruiqi Zhu (朱瑞琦)[1], and Caixia Xu (徐彩霞)[2,*]

[1]*School of Physical Science and Technology, Southwest University, Chongqing 400715, China*
[2]*School of Primary Education, Chongqing Normal University, Chongqing 400700, China*
**Corresponding author: noendness@126.com*

Received March 15, 2020; accepted May 27, 2020; posted online July 31, 2020

The broadband photochromic effect on undoped and rare-earth-doped lead lanthanum zirconate titanate (PLZT) ceramics was studied under the illumination of ultraviolet light at 360 nm. The photocarriers' trapping and detrapping processes of thermal disconnected traps played the vital role in both darkening and bleaching processes. The interaction between photocarrier traps and rare-earth ion energy levels was demonstrated, which influenced the photochromatic darkening performance greatly. The transformation of photoluminescence spectra in Er^{3+}-doped PLZT ceramics also improved the physical picture of the trap's distribution of the materials. This work could be used to modulate the photoluminescence and lasing behavior.

Keywords: photochromic effect; darkening and bleaching process; trapping and detrapping; spectrum transformation.
doi: 10.3788/COL202018.091403.

The photochromic effect is described as a reversible color change of materials driven by photon illumination that could originate from the variation in molecular structure[1,2], evitable oxidation-reduction reactions[3,4], small polarons in crystal lattices[5,6], and also trapping and detrapping in disordered ceramics[7]. When the photochromic effect occurred, refractive index, extinction coefficient, reflection and transmittance of light, and many other optical parameters would also be changed, leading to many potential applications of information storage elements[8], safety protective materials in industrial and automation equipment[9], imaging and display devices[10], and deep ultraviolet detectors[11]. Until now, the photochromic effect has been investigated in a variety of materials including tungsten trioxide (WO_3), titanium dioxide (TiO_2), vanadium oxide (V_2O_5), and many other transitional metal oxide materials[12–16], and also involving diarylethene and spirogyras-based organic materials[17–21]. Recently, Chen *et al.* demonstrated a stable radical formation strategy triggered by photochromism that pointed out a way for the future development of photochemical methodologies and the photomanipulation of advanced optoelectronic materials[22]. Dam's group explored the photochromic properties of YO_xH_y thin films controlled by the lattice compression effect when doped with Zr^{4+} ions[23]. Among all these photochromic materials, lead lanthanum zirconate titanate (PLZT) ceramics was deemed as one of the most promising materials, since they gathered high quadric electro-optical coefficient, and photochromic, pyroelectric, and electrostrictive effects, which was of great interest for designing multifunctional optoelectrical devices[24]. Xu *et al.* exhibited the spectrum transformation in Er^{3+} and Yb^{3+} PLZT by exposing them to the electrical plasma atmosphere[25]. The photochromic effect in Er^{3+}-doped PLZT ceramics with a large-scale refractive index change was investigated, which could be used as a high-performance photodetector in the ultraviolet (UV) region[26]. However, the photochromic interaction between the rare-earth and substrate materials has barely been reported, which is extremely important for modulating the photoluminescence behavior of materials and enhancing the fluorescence efficiency of laser materials. To fill in the gap, in this work, the broadband photochromic effect in undoped PLZT, Er^{3+}-doped, and Nd^{3+} ion-doped PLZT ceramics was studied under the illumination of UV light at 360 nm. The interaction between rare-earth energy levels and thermal disconnected traps was analyzed by comparing the darkening spectrum and absorption peaks. The changes in the absorption coefficient and refractive index were also investigated along with the decreased transmittance of the specimen. The photoluminescence spectrum transformation of Er^{3+}-doped PLZT ceramics was discussed and the physical picture of the spectrum modulation was proposed, which explored a way to modulate the photoluminescence and lasing behavior of this kind of photochromic materials. We reported this work as follows.

A uniaxial hot-press system (Thermal Technology, Model HP52-0914-SC) was used for the ceramic material fabrication. The specimens used in this work were composed of 65 mol% lead zirconate plus 35 mol% lead titanate, and the origins of these components were PbO, ZrO_2, and TiO_2, respectively. To make it transparent, 10 mol% La^{3+} ions in the form of La_2O_3 were added. An excess lead atmosphere was required during sintering to achieve the transparent samples by eliminating the loss caused by the volatility of lead.

The X-ray diffraction spectra of undoped PLZT, 1 mol% Er^{3+}-doped, and 1 mol% Nd^{3+} ion-doped PLZT ceramics were measured by using an X-ray diffractometer (D/MAX-rB, Rigaku, Japan), as seen in Fig. 1(a). The typical cubic perovskite (ABO_3) structure was confirmed with a strong (110) diffraction peak at 30.8°. When Er^{3+}

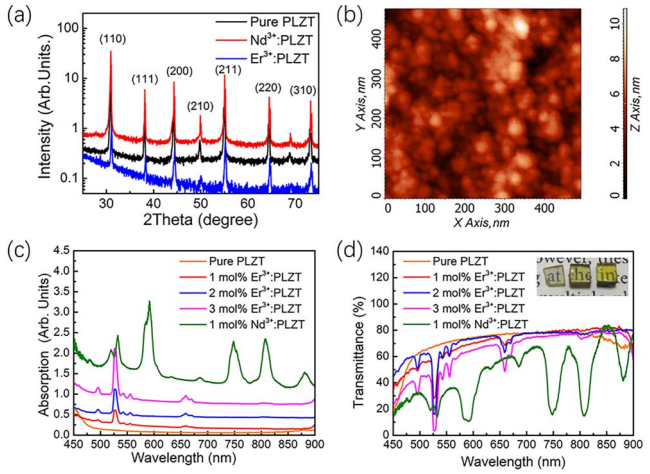

Fig. 1. (a) X-ray diffraction spectrum of undoped PLZT, 1 mol% Er^{3+}-doped, and 1 mol% Nd^{3+}-doped PLZT ceramics; (b) the surface appearance photograph of undoped PLZT ceramics taken by an AFM; (c) the room temperature ground state absorption spectra; and (d) the transmittance spectra of undoped PLZT, 1 mol%–3 mol% Er^{3+}-doped, and 1 mol% Nd^{3+}-doped PLZT samples (the inset is the photograph of the undoped, Er^{3+}-doped, and Nd^{3+}-doped PLZT samples).

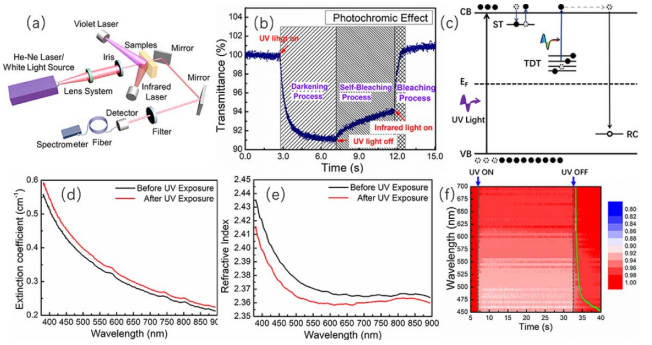

Fig. 2. (a) Schematic illustration of the experimental setup of the photochromic effect; (b) the dynamic change of the transmittance of light in the darkening, self-bleaching, and infrared bleaching processes; (c) the trapping and detrapping process of electrons in TDT; (d) extinction coefficient and (e) refractive index change after UV light exposure; (f) the two-dimensional pseudo color distribution of the transmittance of light at different wavelengths in undoped PLZT ceramics (the inserted green line is the absorption spectrum of undoped PLZT ceramics).

and Nd^{3+} ions were doped into the PLZT ceramics, the diffraction peaks shifted toward larger angles because they replaced the position of Pb at A sites of the structural unit and resulted in a smaller lattice constant and larger diffraction angle. The surface appearance of the undoped PLZT ceramics was analyzed by using an atomic force microscope (AFM), as seen in Fig. 1(b). The grain boundaries varied from grain to grain from several tens to near one hundred nanometers, which was a typical ceramic structure. The roughness of the specimen averaged to be less than 10 nm and it was desirable to make this material highly transparent in the optical direction.

The room temperature ground state absorption and transmittance spectra of undoped PLZT, 1 mol%–3 mol% Er^{3+}-doped, and 1 mol% Nd^{3+}-doped PLZT ceramics were measured, as shown in Figs. 1(c) and 1(d). When Er^{3+} and Nd^{3+} ions were doped into the PLZT ceramics, intensive absorption peaks and transmittance valleys could be seen, referring to the excited absorption of ions from the ground state to the higher energy level of Er^{3+} and Nd^{3+} ions. In this work, these two different energy level structures were used to study the interaction between thermal disconnected traps and rare-earth energy levels during the darkening and bleaching processes.

To study the photochromic effect of the undoped and rare-earth-doped PLZT ceramics, a broadband white light source (200–2700 nm) and a He–Ne laser source (632.8 nm) were used as the signal light to monitor the dynamic change of transmittance through the samples. As drawn in Fig. 2(a), the signal light was collimated by a lens system and confined to a diameter around 0.5 mm by an aperture, and then passed through the transparent surfaces perpendicularly. The intensity of the transmitted light was monitored by the detector and recorded by the oscilloscope or spectrometer. A UV laser at 360 nm and an infrared laser at 790 nm irradiated on the surface of the samples and covered the area of the signal light propagation completely. This was used to activate the darkening and bleaching processes. More optical lenses, irises, and mirrors were ignored in the schematic diagram to focus on the main light path. The transmittance of light dropping rapidly upon the UV laser was enabled and reached equilibrium at the lowest value within several seconds, as exhibited in Fig. 2(b). This darkening process could be explained by the trapping and detrapping of carriers in thermal disconnected traps (TDTs), as illustrated in Fig. 2(c). Electrons on the valence band (VB) were excited into the conduction band (CB) when the light near the bandgap illuminated on surface of the sample, and then combined with the holes in the recombination center (RC) rapidly due to the extremely short lifetime of electrons in the conduction band. During the recombination process, these electrons could be captured by the TDT at a certain probability. When photons propagated through the darkened samples, the captured electrons in the TDT had a chance to be excited to the conduction band and recombine with the holes in the RC again, which also resulted in the darkening phenomenon and reduced the transmittance of light in Fig. 2(b). When the UV light was switched off, both the photons from the signal light and the background could excite part of the electrons in the TDT gradually, leading to a slow rise of the transmitted light intensity [referring to Fig. 2(b)]. The value of the transmittance of light came back to the original value rapidly within several tens of milliseconds after the infrared light was turned on because nearly all the captured electrons were excited to the CB.

Along with the darkening of the samples, both the excitation coefficient and the refractive index could also

be changed, as seen in Figs. 2(d) and 2(e). The excitation coefficient showed an increment of around 0.034 cm^{-1} at 400 nm after being exposed to the UV light at 360 nm, and the increment became smaller in the longer wavelength region (0.010 cm^{-1} at 850 nm). The refractive index of the specimen exhibited an obvious decrease up to 0.02 at 400 nm after being exposed to the UV light at 360 nm, which was an extremely great change and larger than that of many photorefractive single crystals[27–31]. Similar to the change of the excitation coefficient, the reduction of the refractive index was also smaller at longer wavelengths. It was noticeable that it showed an abnormal dispersion from the 700 to 800 nm region [referring to Fig. 2(e)] due to the photoinduced scattering in the disordered structure of this kind of ceramic material[32]. To further study the photochromic effect of the undoped PLZT ceramics, a broadband transmittance variation from 450 nm to 700 nm was measured by the spectrometer (Ocean Optics, USB4000), as exhibited of the 2D pseudo color curves in Fig. 2(e). Analogous to the change of the excitation coefficient and refractive index, the reduction of the transmittance of light was larger at shorter wavelength. Moreover, the recovery time of the transmitted light at shorter wavelengths was also longer since shortwave photons with higher energy were more efficient to excite electrons from the VB to the CB and also had a greater chance to release the captured electrons in the TDT to the CB.

Besides the undoped PLZT ceramics, the photochromic effect of Nd^{3+} and Er^{3+} ion-doped PLZT ceramics samples was also measured to study the interaction between photocarrier traps and rare-earth ion energy levels, which influenced the photochromatic performance greatly. The broadband transmittance variation from 450 nm to 700 nm of 1 mol% Nd^{3+} ion-doped PLZT ceramics specimen was demonstrated in Fig. 3(a); there was also a greater downward trend in the transmittance of light. Compared to the transmittance reduction of the undoped PLZT ceramics sample, it showed a greater decrease that could be lower than seventy percent of the original value. This is because Nd^{3+} ions would replace the position of Pb^{2+} ions at A sites of the perovskite units after they were incorporated into the material, and the number of vacancies was increased due to the unbalance of charges. The increased vacancy concentration lifted up the number of TDTs and the number of captured electrons accordingly. It is noticeable that some abrupt changes occurred near the absorption peak with the decrease of wavelength and enhanced darkening effect due to the interaction of Nd^{3+} ion energy levels with TDTs. The energy distribution of the TDT defects was in a wide range, as seen in Fig. 3(c). The captured electrons interacted with the Nd^{3+} ions in the excited state when they were close to the energy level, and were accompanied by the generation of fluorescence at the corresponding wavelength. The reduced number of captured electrons greatly attenuated the darkening effect. There were some redshifts of the attenuated transmittance of light from the absorption peaks because of the shifts between the absorption and fluorescence peaks.

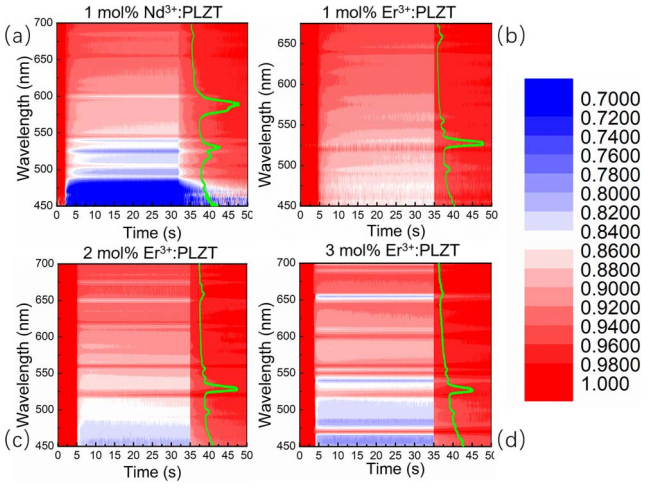

Fig. 3. Two-dimensional pseudo color distribution of the transmittance of light at different wavelengths in (a) the 1 mol% Nd^{3+} ion-doped PLZT ceramics and (b)–(d) the 1 mol%–3 mol% Er^{3+} ion-doped PLZT ceramics.

To verify the interaction between the excited state of rare-earth and captured photocarriers in the TDT, 1 mol%–3 mol% Er^{3+} ion-doped PLZT ceramics samples was prepared and the corresponding two-dimensional pseudo color distribution of the transmittance of light were mapped, as shown in Figs. 3(b)–3(d). Analogical abrupt weakened darkening variation in the change of transmittance of light was also demonstrated near the absorption peaks of the Er^{3+} ions. Based on the analysis above, a more intensive vacancy density inside the sample was formed into the sample with higher Er^{3+} ion concentration. The increased number of captured electrons enhanced the photochromic effect and reduced the transmittance of light subsequently after being irradiated by the UV light. It was pretty obvious that the darkening effect at several wavelengths almost attenuated to disappearance, which originated from the loss of the captured electron by the interaction between the photocarriers in the TDT and the ions on excited state of the Er^{3+} energy level. Moreover, the interaction was extended to the role between the captured electrons and the radiative and nonradiative transition of rare-earth ions, resulting in more abrupt regions in the darkening process.

According to the analysis above, the electrons captured in the TDT played a vital role in the photochromic effect on rare-earth-doped PLZT ceramics, and they interacted with ions in the excited state of the Nd^{3+} and Er^{3+} ions to reduce the decrease in the transmittance of light. To further study the interaction of the captured electrons in the TDT with rare-earth ions, the upconversion process in the visible region and photoluminescence around 1.3–1.9 μm in 1 mol% Er^{3+}-doped PLZT ceramics were investigated. As seen in the inset of Fig. 4(a), a laser diode at 980 nm was used as the pumping source, which was focused by a lens system on the surface of the specimen. The upconverted light emission was collected by another lens system

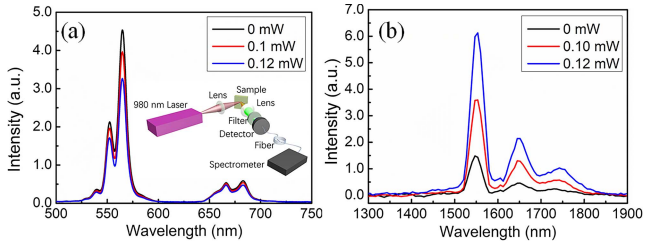

Fig. 4. (a) Upconversion spectra of 1 mol% Er^{3+}-doped PLZT ceramics excited by the laser at 980 nm after being irradiated by UV light at 365 nm with a power of 0 mW, 0.1 mW, and 0.12 mW for 1 min each (the inset is the schematic setup to measure the photoluminescence spectrum); (b) photoluminescence at 1550 nm of 1 mol% Er^{3+}-doped PLZT excited by the laser at 980 nm after being irradiated by UV light at 365 nm with a power of 0 mW, 0.1 mW, and 0.12 mW for 1 min each.

and recorded by a UV-visible-near-IR spectrometer (Ocean Optics, USB4000) and another infrared spectrometer (Ocean Optics, NIR Quest). A 700 nm short pass filter and a 1000 nm long pass filter were used to separate the light emission from pumping light. When the pumping source was switched on, the typical upconversion emission peaks around 528 nm and 539 nm ($^2H_{11/2} \rightarrow {}^4I_{15/2}$), 552 nm and 565 nm ($^2S_{3/2} \rightarrow {}^4I_{15/2}$), and 666 nm ($^4F_{9/2} \rightarrow {}^4I_{15/2}$) emerged instantaneously, accompanied by the infrared fluorescence around 1550 nm ($^4I_{13/2} \rightarrow {}^4I_{15/2}$), as demonstrated in Figs. 4(a) and 4(b)[33]. After the sample was exposed to the UV light at 360 nm for 1 min, both photoluminescence spectra were detected again after the UV light was shut off. The intensity of the upconversion emission peaks went down since these photons were used to release the captured electrons in the TDT, which could be further lowered after being illuminated by a more intensive UV light. Compared with the upconversion emission, the photoluminescence at 1550 nm exhibited a 4-fold enhancement after the UV light exposure. Two main reasons contributed to the enhanced luminescence. 1) The photon energy near 1550 nm was smaller than the energy needed to release the trapped photocarriers from the TDT to the conduction band, and no energy loss was observed during the darkening process. 2) The released photocarriers by the upconverted photons interacted with the energy transition of the Er^{3+} ions, giving rise to an increasing number of ions in the excited state of $^4I_{13/2}$. This result was desirable to design high-power solid-state lasers at 1550 nm because the upconversion loss was suppressed efficiently.

To sum up, a reversible photochromic effect on undoped and rare-earth-doped PLZT ceramics was discussed under the illumination of a UV light source at 360 nm within a broadband range. The model based on photocarriers captured by the TDT and released by photons was responsible for the darkening and bleaching process, respectively. The interaction between the captured electrons and the excited state of the rare-earth ions greatly influenced the photochromic process of the materials, bringing in abrupt attenuations during the darkening process of the wavelength near the absorption peaks and radiative energy transition. With a higher Er^{3+} ion concentration, the darkening process and the interaction between electrons in the TDT and Er^{3+} ions became more intense, which originated from the increased number of vacancies and TDTs with the doping of the Er^{3+} ions. Furthermore, a weakened upconversion emission and an enhanced photoluminescence spectrum were investigated, and the energy loss releasing the trapped electrons in the TDT to the CBs and the interaction between the captured photocarriers and the excited state of the Er^{3+} ions played significant roles in the spectrum transformation. This work provided a way to improve the lasing efficiency of rare-earth-doped solid-state lasers and could also be used to modulate the fluorescence of rare-earth-doped materials and design high-performance optoelectrical devices.

This work was supported by the National Natural Science Foundation of China (NSFC) (Nos. 61805206 and 11804036) and the Fund of China Scholarship Council (No. 201806995045).

References

1. M. Zayat, D. Einot, and R. Reisfeld, J. Sol-Gel Sci. Technol. **10**, 203 (1997).
2. H. Fang, X. Cao, J. Yu, X. Lv, N. Yang, T. Wang, and W. Jiang, J. Mater. Sci. **54**, 286 (2019).
3. M. A. Ashrafi, M. Ranjbar, H. Kalhori, and H. Salamati, Thin Solid Films **621**, 220 (2017).
4. X. G. Hu, X. L. Li, S. H. Kim, K. H. Ahn, and S. I. Yang, Dyes Pigm. **172**, 107869 (2020).
5. S. Cao, F. Gao, J. Xu, J. Zhu, Q. Che, Y. Guo, L. Li, J. Liu, and T. Gao, J. Eur. Ceram. Soc. **39**, 5260 (2019).
6. M. Lee, S. Takekawa, Y. Furukawa, Y. Uchida, K. Kitamura, H. Hatano, and S. Tanaka, J. Appl. Phys. **88**, 4476 (2000).
7. K. Tanaka, Y. Hamakawa, K. Waking, and M. Murata, J. Am. Ceram. Soc. **59**, 465 (1976).
8. D. J. Wales, Q. Cao, K. Kastner, E. Karjalainen, G. N. Newton, and V. Sans, Adv. Mater. **30**, 1800159 (2018).
9. L. Liu, Y. Ren, J. Pan, Z. Liu, B. Wu, and F. Yan, ACS Appl. Mater. Int. **12**, 1495 (2019).
10. W. Yang, D. Wu, R. Wu, G. Liu, B. Chen, L. Feng, Z. Zhang, and A. Wang, Chin. Opt. Lett. **17**, 071405 (2019).
11. A. Ranjkesh, M. K. Park, D. H. Park, J. S. Park, J. C. Choi, S. H. Kim, and H. R. Kim, Sensors **16**, 38 (2016).
12. C. Bechinger, G. Oefinger, S. Herminghaus, and P. Leiderer, J. Appl. Phys. **74**, 4527 (1993).
13. I. Paramasivam, J. M. Macak, A. Ghicov, and P. Schmuki, Chem. Phys. Lett. **445**, 233 (2007).
14. J. Gomez-Hermoso-de-Mendoza, H. S. Barud, J. Gutierrez, and A. Tercjak, Carbohydr. Polymer. **208**, 50 (2019).
15. T. He and J. Yao, J. Photochem. Photobiol. C **4**, 125 (2003).
16. N. Couzon, M. Maillard, L. Bois, F. Chassagneux, and A. Brioude, J. Phys. Chem. C **121**, 22147 (2017).
17. S. Pu, C. Zheng, Z. Le, G. Liu, and C. Fan, Tetrahedron **64**, 2576 (2008).
18. Y. Ishiguro, R. Hayakawa, T. Chikyow, and Y. Wakayama, J. Mater. Chem. C **1**, 3012 (2013).
19. T. Chen, Z. Sun, S. Zhao, C. Ji, and J. Luo, J. Mater. Chem. C **4**, 266 (2016).

20. A. G. Lvov, A. M. Kavu, V. V. Kachala, Y. V. Nelyubina, A. V. Metelitsa, and V. Z. Shirinian, J. Org. Chem. **82**, 1477 (2017).
21. C. B. Fan, L. L. Gong, L. Huang, F. Luo, R. Krishna, X. F. Yi, A. M. Zheng, L. Zhang, S. Z. Pu, X. F. Feng, and M. B. Luo, Angew. Chem. Int. Edit. **56**, 7900 (2017).
22. X. Chen, W. Zhao, G. Baryshnikov, M. L. Steigerwald, J. Gu, Y. Zhou, H. Ågren, Q. Zou, W. Chen, and L. Zhu, Nat. Commun. **11**, 945 (2020).
23. F. Nafezarefi, S. Cornelius, J. Nijskens, H. Schreuders, and B. Dam, Sol. Energy Mater. Sol. Cells **200**, 109923 (2019).
24. G. H. Haertling, Ferroelectrics **75**, 25 (1987).
25. L. Xu, J. Zhang, S. Zhang, C. Xu, Y. K. Zou, and H. Zhao, J. Appl. Phys. **113**, 223101 (2013).
26. C. Xu, J. Zhang, L. Xu, and H. Zhao, J. Appl. Phys. **117**, 023107 (2015).
27. N. V. Sidorov, M. N. Palatnikov, N. A. Teplyakova, A. A. Gabain, and I. N. Efremov, Opt. Spectrosc. **120**, 633 (2016).
28. X. Wang, X. Yan, K. Jin, Y. Dai, Z. Jin, X. Yang, and G. Ma, Chin. Opt. Lett. **17**, 113201 (2019).
29. L. I. Ivleva, N. V. Bogodaev, N. M. Polozkov, and V. V. Osiko, Opt. Mater. **4**, 168 (1995).
30. L. Xu, C. Xu, H. Sun, T. Zeng, J. Zhang, and H. Zhao, ACS Photon. **5**, 4463 (2018).
31. K. Kitamura, Y. Furukawa, Y. Ji, M. Zgonik, C. Medrano, G. Montemezzani, and P. Günter, J. Appl. Phys. **82**, 1006 (1997).
32. L. Xu, J. Zhang, C. Xu, and H. Zhao, J. Lumin. **173**, 185 (2016).
33. F. Shi, M. Zhao, C. Jia, Y. Zhao, and S. Chen, Chin. Opt. Lett. **16**, 011403 (2018).